SCI. MAR., 56(4): 357-366 SCIENTIA MARINA 1992

Sea surface mesoscale structures imaged by the synthetic aperture radar*

ANTONIO MARTÍNEZ[1], JORDI FONT[1], VICTORIANO MORENO[2] and EMILI GARCÍA[3]

[1]Institut de Ciències del Mar, CSIC, P.° Nacional s/n. 08039 Barcelona, Spain
[2]INISEL ESPACIO, Av. Burgos, 8 bis, 3.ª planta, 28036 Madrid, Spain
[3]Dep. Física, Universitat Autònoma de Barcelona, 08193 Bellaterra, Spain

SUMMARY: The synthetic aperture radar (SAR) is an active sensor working in the frequency range of the microwaves. Its distinctive characteristic is the synthesis of a large antenna through the study of the phase of the received pulses over an integration time. The possibility of producing high resolution images regardless of the weather conditions makes SAR a very suitable sensor for the remote sensing of the ocean surface. In this paper we present the main characteristics of SAR, several techniques of image processing, and its applications to the study of sea surface structures, especially those related to mesoscale currents. We describe one of the first SAR images acquired by the European ERS-1 satellite in 1991 in the western Mediterranean.

Key words: Physical oceanography, surface layer currents, microwave remote sensing, SAR, ERS-1.

RESUMEN: OBSERVACIÓN DE ESTRUCTURAS DE MESOESCALA EN LA SUPERFICIE DEL MAR MEDIANTE EL RADAR DE ABERTURA SINTÉTICA. — El radar de abertura sintética (SAR) es un sensor activo que trabaja en el intervalo de frecuencias de las microondas. Su característica distintiva es la síntesis de una antena de grandes dimensiones mediante el seguimiento de las fases de los pulsos recibidos durante un tiempo de integración. La posibilidad de producir imágenes de alta resolución con independencia de las condiciones meteorológicas hacen del SAR un sensor muy atractivo para la observación remota del océano. En este trabajo se presentan las características del SAR, las técnicas de proceso de sus imágenes y sus aplicaciones al estudio de estructuras superficiales del mar, especialmente aquellas ligadas a la variabilidad de mesoescala de la circulación. Se describe una de las primeras imágenes SAR obtenidas en 1991 por el satélite europeo ERS-1 en el Mediterráneo occidental.

Palabras clave: Oceanografía física, corrientes superficiales, teledetección por microondas, SAR, ERS-1.

INTRODUCTION

Spaceborne remote sensing is now an usual tool in oceanographic research. Infrared images of the sea surface are widely used to complement *in situ* data in coastal and open ocean circulation studies. Temperature is used as a tracer, and surface circulation-related structures are associated to water masses of different temperature. Satellite infrared radiometers permit a synoptic view of a large area at a spatial resolution of about 0.5 km, and in combination with irregularly available, non-synoptic *in situ* data, it offers opportunities for improved data interpretation. Other passive sensors, like visible wavelength radiometers, are also relevant for coastal areas and biological investigations.

In 1978 SEASAT was the first satellite to carry active microwave instruments (radars) to sense the sea surface. Although only three months of data were generated, the enormous capacity of these new sensors for oceanographic research became immediately evident. Later on, radar altimeters have been largely operational (GEOSAT) or recently launched (TOPEX/POSEIDON) in ocean topographic missions. A complete package of active microwave instruments in the first European Remote-Sensing Satellite (ERS-1) makes it the "forerunner of a new genera-

* Received July 17, 1992. Accepted October 20, 1992.

tion of space missions planned for the 1990s in the domain of the environment" (P. Goldsmith, Director of Observation of the Earth and Its Environment, European Space Agency).

The Synthetic Aperture Radar (SAR) is an active sensor, working in the frequency range of the microwaves. The main distinctive characteristic of SAR is the synthesis of a large antenna from an actually small one, through the study of the phase of the received pulses over an integration time. The possibility of producing high resolution images regardless of the external ilumination and weather conditions makes SAR an attractive imaging device for the remote observation of the Earth. The recent launching of ERS-1, Japanese JERS-1 and Russian ALMAZ 1, and the forthcoming USA's SIR-C and Canadian RADARSAT SARs confirm this fact.

In this paper we present the SAR operational principles, its comparison with optical and infrared sensors, and several correction techniques for the processing of SAR images: the reduction of the speckle noise and the transformation from slant to ground range geometry. The application of SAR imagery to oceanographic studies is reviewed and one of the first ERS-1 SAR images of the Mediterranean Sea is presented. This study is part of the project "Evaluation of ERS-1 microwave sensors capability in the study of oceanic fronts" approved by the European Space Agency.

THE SYNTHETIC APERTURE RADAR

The first and fundamental difference between radars and optical or infrared sensors is the electromagnetic radiation used. Visible wavelength is in the order of 0.5 μm, infrared, 10 μm, and radar 10 cm. This gives rise to the observation of different properties of the targets, and consequently, an additional information source. The surface properties that affect the microwave scattering are the electrical characteristics, the roughness and the geometric shape; radar parameters as the wavelength, incidence angle and polarization are also responsible for the response. The higher penetration (lower losses) in the atmosphere of the microwaves is a main advantage, as it allows to work independently of the cloud cover. On the other hand, the active nature of radar sensors means the non dependence on external illumination.

Among the various radar systems the only with imaging capabilities useful for remote sensing are the Side-Looking Radars (SLR), and among them, the Synthetic Aperture Radar is the most important one, due to its higher spatial resolution in particular obtained in azimuth (along track) direction. A side-looking radar is essentially a long antenna mounted on board an aircraft, parallel to the motion direction. The antenna emits short microwave pulses perpendicular to its main axis. These pulses, after reflecting on the ground, are received by the same antenna, and ordered according to the delay time between emission and reception; that is, as a function of the distance from the target to the antenna.

The spatial resolution of a SLR is restricted by the pulse and antenna lengths. In order to improve the ground resolution, both in azimuth and range, several modifications to this simple scheme have to be made, leading to the SAR. The range resolution can be improved by compressing the electromagnetic pulse (reducing the pulse length). In azimuth direction the situation is somehow different: as the antenna reaches and passes by a target on the ground, the frequency of the reflected radiation will be shifted by Doppler effect, due to the varying relative velocity between antenna and target. The principle under the SAR is to synthesise a long antenna by processing not only the delay of the received echoes, but also their frequency and phase. So, the emitted radiation must be coherent (with defined, and known phase).

At a given time and distance from the antenna, the contribution of each ground point, in the along track direction, can be distinguished taking into consideration the frequency's Doppler shift. This differentiation is performed in practice by filtering the received signals with a reference pulse. The frequency of the reference pulse is adjusted according to the Doppler history of the ground point being processed. The filtered pulses are then added or integrated coherently during the synthetic aperture time. In this way it is possible to integrate separately the contributions from different points on the ground. It is surprising that the resulting azimuthal resolution is independent of the distance from antenna to target.

PROCESSING SAR IMAGES

The use of remotely sensed information in oceanography requires the development of several image processing techniques. Working with SAR, besides some common aspects with other sensors (e. g. geometric distortions), poses specific problems that are now under study. The large amount of data contained in the full-resolution SAR images makes unavoidable

the need for specific processing facilities, efficient data management and filtering techniques.

One of the distinctive characteristics of SAR imagery is the presence of typical noise pattern, known as speckle. The speckle noise is originated in the scattering of the incidence radar pulse by a great number of scatterers within each resolution cell. The random orientation of these elements makes the phases of the dispersed pulses change. As the reflected pulse is the coherent sum of the different contributions from the elements within the resolution cell, there will be constructive and destructive interference when the pulses are in or out of phase. Assuming a big number of scatterers within a resolution cell, the noise statistics can be modelled by a normal distribution with mean value 1 and variance 0.52. This result is commonly called the speckle multiplicative model (ULABY *et al.*, 1986).

The multi look processing is usually used to reduce the speckle noise. This technique consists in averaging several looks (four in the case of SEASAT and three for ERS-1) in the azimuth direction. In this way, the standard deviation of the noise will be reduced by a factor of $n^{1/2}$, being n the number of averaged looks. The multi look process also allows to obtain almost the same pixel size in azimuth and range directions (usually the azimuthal resolution, and so the azimuth pixel size, is lower than the corresponding in the range direction). The standard deviation of a four looks amplitude image is about 0.26 (for homogeneous areas). Further reduction of this deviation will improve the visual appearance of the image and also will make easier the following processes such as edge detection, segmentation or classification.

Several filters for speckle reduction can be found in the literature. We have implemented and studied three of them. Let's remember that the ideal behaviour of a speckle filter is to reduce as much noise as possible while keeping textural and edge information untouched. This is the reason for not to use a simple averaging filter as it does not preserve this information.

The median filter substitutes the value of each pixel by the median of the pixel values located within a window centred on the reference pixel. The window size is usually set to 3×3 or 5×5. The performance of the median filter is higher than that of the mean filter, as it preserves better the edges between adjacent areas. The extreme values have less influence in the determination of the median than in the mean, and its similarity to the mean value of the majority of the pixels in the window is the reason for its superiority over the averaging filter. The median filter is easy to implement, and is widely used (JOHANNESSEN and SKAGSETH, 1988).

The sigma filter is, in essence, an averaging filter. The difference between the sigma and the simple mean is that the former does not include necessarily all the pixels in the window for the calculation of the final value. The only pixels considered are those whose amplitudes are between plus or minus two standard deviations (sigmas) of the central pixel value (LEE, 1983). With this modification it is intended to group the pixels from different regions into different populations, in order not to lose edge information. The main assumption under the sigma filter is the normal distribution of the values of the pixels belonging to the same region.

The statistical filter is a different approach to the speckle reduction problem. In this case it is intended to create a filter in which the final pixel value is based on the local characteristics of the image (adaptive filter). The filtered value is calculated using (LEE, 1981):

$$s_f = s_m + \frac{\delta(s)}{s_m^2 \sigma_v^2 + \delta(s)} (s - s_m) \quad (1)$$

where:

- s is the original pixel value at the centre of the window
- s_m is the mean value in the window
- $\delta(s)$ is the variance in the window
- σ_v is the speckle standard deviation
- s_f is the final value of the pixel

Studying equation 1 it is possible to follow the behaviour of the filter in two extreme cases. In homogeneous areas s should be equal to s_m, and the filtered value will be the mean value over the window ($s_f = s_m$). When the region is strongly heterogeneous, that is, there is an edge or a point target, the variance of the pixel values in the window should be much greater than the speckle deviation ($\delta(s) >> s_m \sigma_v^2$) and the final filtered value will be the original pixel value.

The application of the three implemented filters with varying window sizes shows that the election of the ideal filter is dependent on the scene been analyzed. In general, it seems that the statistical filter with a 5×5 window offers the best results.

SAR images, as those from other remote sensors, are subjected to different geometric distortions. It is needed to correct these distortions in order to relate the image pixels to an external reference or coordinate frame. The geometric correction of SAR images is generally performed from the data in the satellite

ephemerid. In this way it is possible to avoid the dependence on ground control points.

The first step in the geometric calibration of a SAR image is the location of the pixels. This task is performed by solving the two equation leading the image formation process: the equations defining the ground points placed at a given distance from the antenna and the equation of the points having the same Doppler frequency shift. The condition that the image points are on the Earth surface has to be also entered. Usually, the Earth shape is assumed to be a spheroid. The orientation, position and velocity of the antenna have to be known before solving the equations. The rotational speed of the Earth adds an extra Doppler shift in the received signals; usually this effect is corrected for in the on board processor, but the used Doppler offset, or its corresponding squint angle, is needed for solving the geometrical model.

The panoramic distortion is typical of radar imagery. As commented before, the axis of the SAR coordinate system are azimuth, along the flight line, and range, across track. The range direction is not parallel to the surface, as it is the projection of the distance from target to antenna. The task of reconstructing a SAR image has to include the projection of these distances on the ground. This process is commonly referred to slant to ground range transformation. The relationship between the slant and ground pixel sizes is:

$$\delta_g = \frac{\delta_s}{\sin\vartheta} \qquad (2)$$

where:

δ_s is the slant range pixel size
δ_g is the ground range pixel size
ϑ is the incidence angle

The original pixel spacing (in slant range) is constant, because the received pulses are sampled at constant times (sampling frequency). So, the resulting ground pixels will have a varying size along the image. From equation 2 it is seen that the slant range image is compressed in the range direction; the compression factor is bigger when the distance from target to antenna is smaller (in the near range zone, where the incidence angles are smaller).

The development of these filtering and correction tools has been implemented with two SEASAT SAR scenes of the western Mediterranean provided by the European Space Agency, as a preliminary stage of the processing of ERS-1 SAR images.

SAR IMAGES OF THE OCEAN

A SAR image of the ocean represents the magnitude of the radar energy backscattered in its surface. The radar illumination is oblique, and so, the specular reflection will not be the main mechanism of interaction between the radar waves and the sea surface; it will be the Bragg scattering, due to the surface roughness. It is important to point out that the radar waves do not penetrate in the sea more than a few milimetres, so the features observed in SAR images correspond to surface phenomena.

The main interaction mechanism between the sea surface and the incident microwave radiation is, for the side looking radar, the modulation of the pulses by short gravity waves via Bragg resonant scattering when the sea state is moderate (VALENZUELA, 1978; WRIGHT, 1978). It is well established that the radar waves interact more strongly with surface modulations with similar length to the incident wave length. The problem is much more complex when dealing with SAR imatges, because it is needed to include the motion of the waves during the integration or aperture time (ALPERS and RUFENACH, 1979). There are a number of proposed models, with limited applications, that are now under discussion in this field of current research (HASSELMANN *et al.*, 1985).

Some marine processes modulate the energy of the wind generated waves, that are the responsible for the roughness of the sea surface that interacts with the radar waves. This modulation is translated in the image to areas with different textures and intensities, that will be related to the structure and nature of the corresponding marine phenomenon and also to the spatial variation of the wind stress (BEAL *et al.*, 1981; VESECKY and STEWART, 1982).

Among the surface marine processes that can be observed in SAR imagery there are the long gravity waves and the variable currents associated to hydrographic structures, such as fronts and eddies. Several subsurface phenomena can be observed as well, such as internal waves and variations in the bathymetry, due to their effects in the roughness of the marine surface. In addition to these oceanographic processes, other structures can appear in SAR images of the sea surface due to the variability of the local wind field, changes in the atmospheric boundary layer stratification or to the presence of polluted or natural slicks.

Internal waves are propagating perturbations produced in the interphase between different water masses, and lead to the formation of convergent and divergent flux areas in the surface. These areas affect

the pattern of the waves and, consequently, the roughness of the sea. In the case of shallow waters, a strong current along a variable depth can produce vertical motions that will be reflected as alterations in the surface.

Marine fronts are boundaries between water masses with different physicochemical characteristics (mainly temperature and salinity) under equilibrium in a strong density gradient. Besides the difference in roughness across the fronts, they are zones of surface convergence, leading in some cases to the formation of wave breaking or even accumulation of detritus. The frontal regions are dynamically very active, with the development of surface structures such as eddies and filaments. Their relationship with the currents' pattern and their extended dimensions are two reasons that encourage the use of SAR imagery in their study.

During the summer of 1978, several observations of marine fronts and eddies in SEASAT SAR images were reported (FU and HOLT, 1983; ALLAN and SCOON, 1986). Preparatory studies before the ERS-1 launching have stated the feasibility of the distinction between marine fronts and other features detected in images of the sea surface directly related to the wind. JOHANNESSEN *et al.*, (1991), with an airborne C band SAR during the Norwegian Continental Shelf Experiment in March 1988 (NORCSEX'88), identified frontal mesoscale current shear as narrow bright lines in the backscatter.

ANALYSIS OF ERS-1 IMAGES OF THE BALEARIC SEA

The first European Space Agency (ESA) remote sensing satellite (ERS-1) was successfully launched on 17 July 1991 into a 780 km polar orbit. It is equipped with an active microwave instrument package that contains a C band SAR capable of providing a resolution on the ocean surface of about 30 m. The swath width on ground is 100 km and the radar incidence angle is 23°. After completing all the instrument engineering performance tests the SAR was declared operational by ESA in mid October 1991.

In November a field experiment (NORCSEX'91) was carried out by the Nansen Environmental and Remote Sensing Centre (Bergen, Norway) to validate the ERS-1 SAR imaging capabilities of several near-coastal phenomena, under weather conditions ranging from moderate to extreme. One of the main results was to distinguish and classify three different kinds of surface structures in SAR imagery (JOHANNESSEN *et al.*, 1992a): wind fronts (step-like transition zone from low to high backscatter intensity), current shear in marine fronts or eddies (peak-like backscatter change) and internal wave trains (crest/trough, regularly spaced bright and dark backscatter zones). The clear expression of the oceanic features in SAR images is limited by both high and low wind speeds (4 to 10 m/s). Furthermore, good correspondence has been found between eddies detected by ERS-1 SAR through the presence of slicks and simulated in a non-linear reduced gravity model in the western coast of Norway (JOHANNESSEN *et al.*, 1992b), that demonstrates the possibility of using SAR data together with models for the monitoring of mesoscale coastal processes.

A research project, conducted by several Spanish and British institutions, aims at developing methods to extract the identification of mesoscale frontal features from ERS-1 SAR images and altimeter data, and to evaluate its sensitivity under different conditions in the western Mediterranean. "Evaluation of ERS-1 microwave sensors capability in the study of oceanic fronts", coordinated by the Institute of Marine Sciences, Barcelona, was accepted by ESA as a response to the ERS-1 Announcement of Opportunity issued in 1986. The project will have access to a total of 50 SAR images and the whole altimeter data set, and participates in the planning of sensor operations to coordinate the field work with SAR data acquisition. The western Mediterranean provides a large variety of evolving mesoscale structures that can be sampled with relative low cost and difficulties, thus permiting to test the usefulness of ERS-1 sensors to operate in other remote oceans.

As indicated above, a first step of the project was the development of computer tools for the treatment of SAR images (MARTÍNEZ *et al.*, 1992). Fig. 1 shows one of the SEASAT SAR images used in that phase. It corresponds to the southern part of the Italian peninsula (Calabria) and the strait of Messina, separating it from Sicily, as well as a coastal area of the Thyrrenian Sea. The spatial resolution is 25 m. This image has been studied in detail by ALPERS and SALUSTI (1983). It presents a dark zone in the north (low radar backscatter), that corresponds to a damping of the surface roughness due to strong turbulence typical of that area. Internal wave solitons, generated in the strait of Messina, are observed propagating northward near the transition to the low backcatter region. Other remarkable features are coastal waves in the centre of the image, and typical tidal bores within the strait.

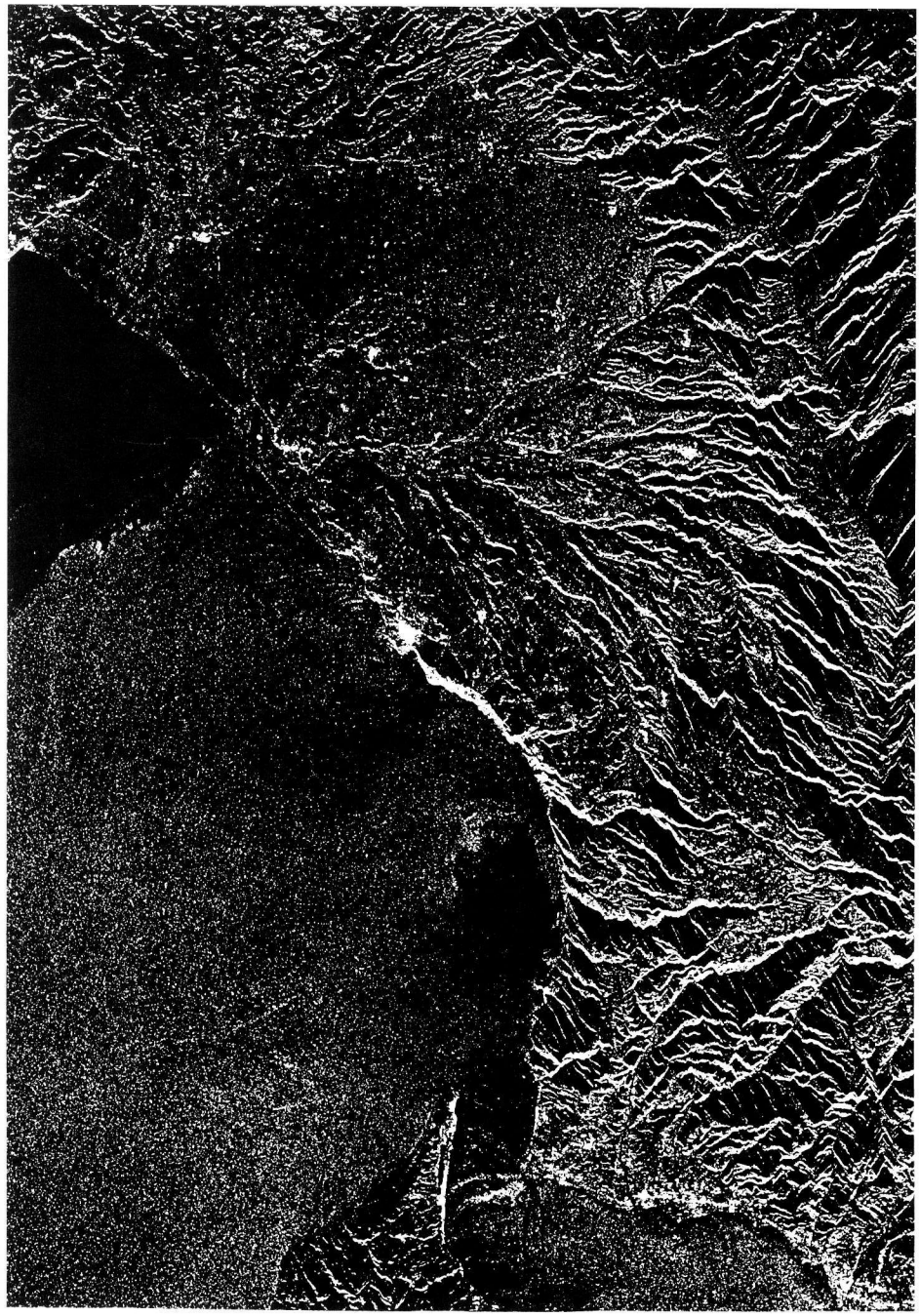

FIG. 1. — Full resolution (25 m) ground range SEASAT SAR image of the strait of Messina and southeastern Thyrrenian Sea, acquired on 15 September 1978. Processed by DFVLR/GSOC for ESA/Earthnet.

During its Phace A (July to December 1991) ERS-1 was set in a 3-day repeat cycle to allow for calibration activities. One of the areas covered by the SAR swath during this phase was the Balearic Sea between Ibiza island and the Ebro river delta (Fig. 2). The circulation in this region is controlled by two density fronts that follow the peninsular and insular continental slopes (FONT *et al.*, 1988; LA VIOLETTE *et al.*, 1990; CASTELLÓN *et al.*, 1990). One of the characteristics of these fronts is that they are due mainly to salinity, not to temperature, so we expected to find SAR specially useful to identify frontal structures that can be hidden to infrared radiometers. The peninsular frontal region (Catalan front) results to be dynamically active, generating eddies and filaments that have been observed both by *in situ* and infrared satellite data (WANG *et al.*, 1988; TINTORÉ *et al.*, 1990), due to the presence of a cold water vein (from the Gulf of Lions) entrained in the alongslope current.

A cruise was planned to cover the shelf and slope

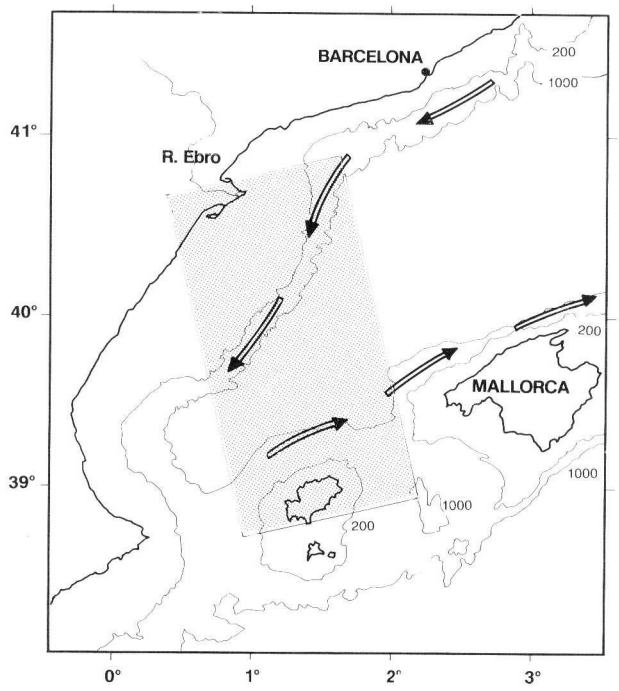

FIG. 2. — Location of the ERS-1 SAR pair of images in the Balearic Sea. The direction of the frontal Catalan and Balearic currents are indicated along the continental slope.

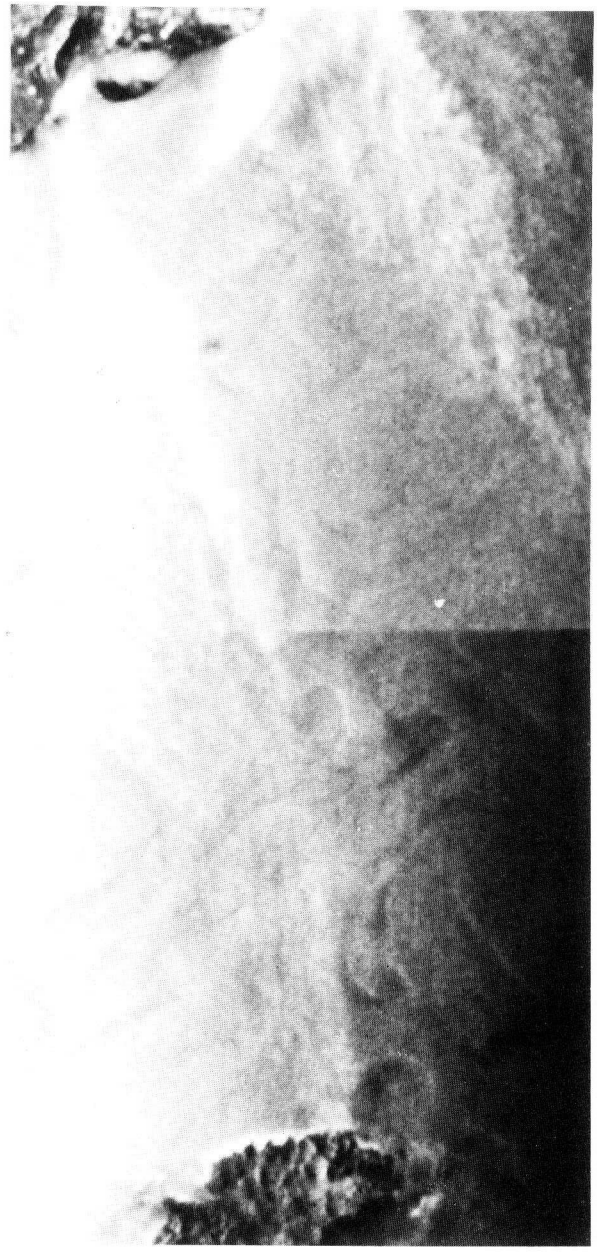

FIG. 3. — Mosaic of two consecutive low resolution (400 m) SAR scenes, acquired by ERS-1 at 22 GMT on 20 November 1991. Copyright ESA 1991. ERS-1-R.

area off the Ebro delta during the ERS-1 passage, including the sampling of the three dimensional density (CTD probe) and velocity (ADCP) fields. The temperature field had to be measured in a wider region by means of AXBTs dropped from a plane. Unfortunately, a last moment delay of three months in ERS-1 launch did not permit to modify the ship schedule and acquire SAR images simultaneously to the oceanographic data (May-June 1991, SALAT *et al.*, 1992).

The area was finally imaged by ERS-1 on November 1991. Figure 3 is the first SAR image (two consecutive scenes) provided by ESA, including half of the Ebro delta and the island of Ibiza. The original spatial resolution (20 m in range, 16 m in azimuth) has been reduced to 400 m in order to display simultaneously the two scenes. No radiometric correction has been applied. Although the lack of field measurements does not allow a direct comparison, some features can be inferred in the image. It has not been possible to contrast it with NOAA infrared pictures, due to the extensive cloud cover in the region when the SAR image was acquired.

Near the delta, one can distinguish the main river discharge (plume) and some lateral discharges in the southern bay. The plume is bending to the alongshore direction, that is following the alongslope circulation dominant in the area (FONT, 1990). We cannot identify the long structure that crosses the image at a near northwest-southeast direction. It coincides with the general directon of surface isotherms compiled from NOAA AVHRR for the week 22-28 November (SATMER, 1991), but these thermal values do not reveal any significant gradient in that location. The structure could be related to wind, since strong northwesterlies, flowing along the Ebro valley, are typical in autumn and reach the coastal sea after having been

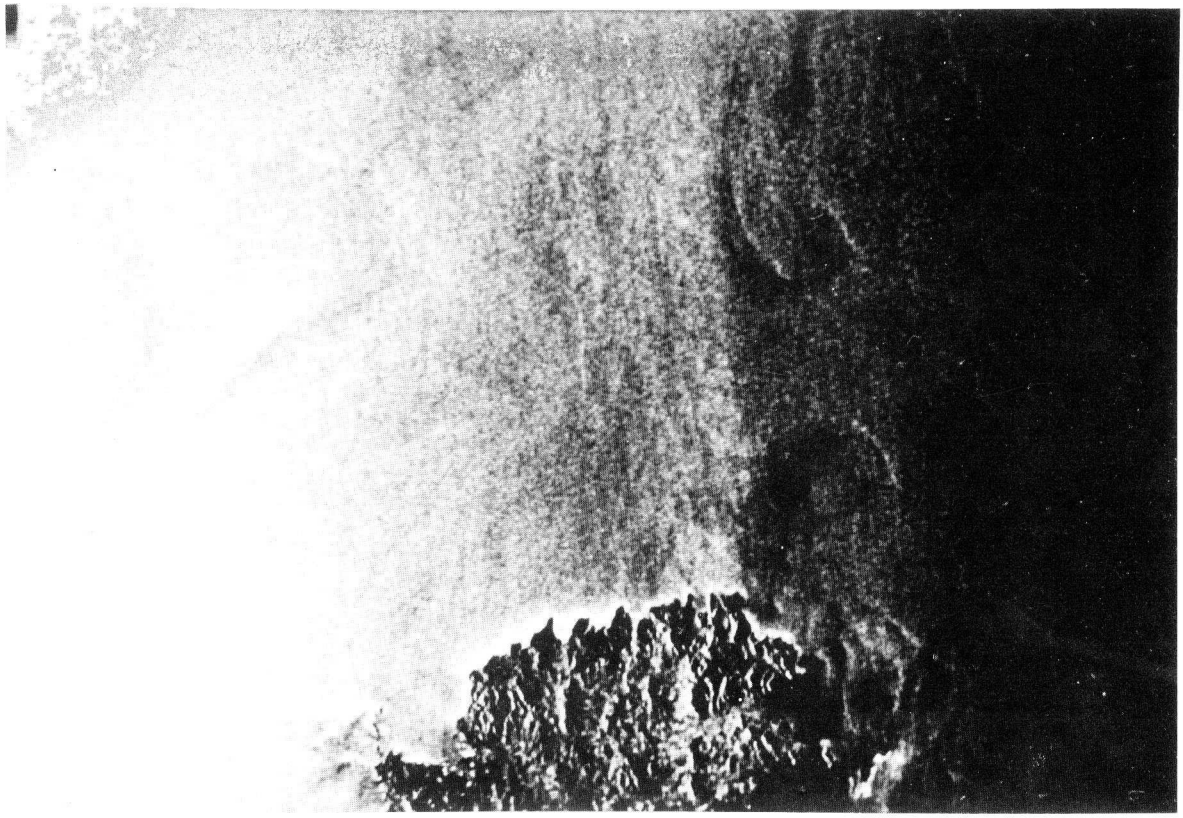

FIG. 4. — Mesoscale structures near Ibiza imaged by SAR. Enlargement at higher resolution of the southern part of Fig. 3. Copyright ESA 1991. ERS-1-R.

channelled in the narrow lower valley. At the time of the image wind from 310°-350° had been recorded near the mouth of the delta for several days, and was above 10 m/s for the last 6 hours. In any case this structure does not correspond to a surface circulation signature and even, near the island, it intersects, at an almost right angle, other features that are clearly in the direction of the current. A second structure in the NE corner, parallel to the first one, has a different texture and seems to originate in the gulf north of the delta. It could also have something to do with the wind, or reflect the interaction of the alongslope current with the local topography, as it has been observed there in other occasions in autumn, with near-surface isopycnals aligned in this direction (FONT *et al.*, 1990).

The image does not give any evidence of the jet-like current that is associated to the Catalan front (see in LA VIOLETTE *et al.*, 1990, its signature in AVHRR images). There are two possible reasons for this: the existence of a fully developed surface mixed layer (usually down to 40-50 m at the end of the stratified season, before the autumn erosion of the thermocline) keeps the main current system below the surface structures detected by remote sensing (LÓPEZ *et al.*, 1992). The second reason is that in the area covered by the SAR image, downstream the Ebro delta, the alongslope current has been observed in several occasions to be detached from the slope and interacting with surface water flowing from the south, thus giving rise to a less defined circulation pattern (CASTELLÓN *et al.*, 1990; SALAT *et al.*, 1992).

In the southern part of the image several lines appear in the direction of the current associated to the Balearic front. Just in that area, north of Ibiza, is where the front is formed due to the less dense waters that are incoming through the channels at both sides of the island. Direct current measurements and hydrographic data (GARCÍA *et al.*, 1991) describe the formation of the alongfront current in the direction indicated by the shear lines observed in the SAR image.

Probably the most striking feature in the image is the very clear presence of mesoscale eddies northeast of Ibiza. Fig. 4 is an enlargement of this part of the image, with a resolution of 80 m in range and 64 in azimuth. One of the eddies is close to the island, while the other seems to be part of a mushroom-like dipole structure originated in the middle of the channel that separates Ibiza from Mallorca. Such king of

structures have been observed in infrared images associated to the current in the Catalan front (LA VIOLETTE *et al.*, 1990), although here the lengths are smaller (40 km the head of the mushroom, less than 10 km the diameter of the eddies). These eddies reflect the mesoscale activity associated with the dynamics of the incoming water. Recent studies with infrared NOAA imagery (LÓPEZ *et al.*, 1992) have revealed that this area is much more active than previously estimated. The above mentioned NOAA sea surface temperature weekly compilations (SATMER, 1991) indicate frontal structures coincident with those shear lines, and especially with the western edge of the two-eddies system.

This first ERS-1 SAR image is a good example of the detection of mesoscale structures that can be achieved in the western Mediterranean. Although the lack of contemporaneous oceanographic data has not allowed an adequate identification of the detected features, it is clear that mesoscale phenomena related to the surface currents are perfectly imaged. Our project will continue to develop analysis tools and perform the SAR/*in situ* comparison under different situations.

The next step is the joint analysis of the data collected in three oceanographic surveys (May-June 1992) in a coastal submarine canyon area north of Barcelona, and five ERS-1 SAR images acquired during this period. Then a major experiment will take place next autumn in the Alboran Sea, with intensive oceanographic sampling together with current measurements that will be integrated in a study of a large set of ERS-1 SAR and altimeter data.

ACKNOWLEDGEMENTS

This study is funded by the Spanish National Program on Marine Resources (project MAR89-0550) and by INISEL ESPACIO through a research contract with CSIC. All the SAR images have been provided by the European Space Agency. ERS-1 SAR data are used according to the agreement signed by CSIC to the terms and conditions defined by ESA. The work with SEASAT images was done in cooperation with the Department of Oceanography of the University of Southampton.

REFERENCES

ALLAN, T. D. and A. SCOON, — 1986. Study of the Iceland-Faroe oceanic front by Seasat's SAR. *Institute of Oceanographic Sciences, UK.*

ALPERS, W. and C. L. RUFENACH. — 1979. The effect of orbital motions on SAR imagery of ocean waves. *IEEE Trans. Ant. Propagat.*, AP-27: 685-690.

ALPERS, W. and E. SALUSTI . — 1983. Scylla and Charybdis observed from space, *J. Geophys. Res.*, 88(C3): 1800-1808.

BEAL, R. C., P. S. DELEONIBUS and I. KATZ, (eds.). — 1981. *Spaceborne Synthetic Aperture Radar for oceanography.* Johns Hopkins Univ. Press, Baltimore, USA, 216 pp.

CASTELLÓN, A., J. FONT and E. GARCÍA. — 1990. The Liguro-Provençal-Catalan current (NW Mediterranean) observed by Doppler profiling in the Balearic Sea. *Sci. Mar.*, 54(3): 269-276.

FONT, J. — 1990. A comparison of seasonal winds with currents in the continental slope of the Catalan Sea (NW Mediterranean). *J. Geophys. Res.*, 95(C2): 1537-1546.

FONT, J., J. SALAT and J. TINTORÉ. — 1988. Permanent features of the circulation in the Catalan Sea. *Oceanol. Acta*, vol. sp. 9: 51-57.

FONT, J., J. SALAT and A. JULIÀ. — 1990. Marine circulation along the Ebro continental margin. *Mar. Geol.*, 95: 165-177.

FU, L. L. and B. HOLT. — 1983. Some examples of detection of oceanic mesoscale eddies by the SEASAT Synthetic-Aperture Radar. *J. Geophys. Res.*, 88(C3): 1844-1852.

GARCÍA, E., A. CASTELLÓN and J. SALAT. — 1991. Some features of the Balearic front in June 1989. *XX Gen. Assem. IUGG-IAPSO*, PS04: 65.

HASSELMANN, K., R. K. RANEY, W. J. PLANT, W. ALPERS, R. A. SCHUCMAN, D. R. LYZENGA, C. L. RUFENACH and M. J. TUCKER. — 1985. Theory of Synthetic Aperture Radar ocean imaging: a MARSEN view. *J. Geophys. Res.*, 90(C3): 4659-4686.

JOHANNESSEN, J. A. and O. SKAGSETH. — 1988. *Feasibility of the use of SAR data to quantify variations in backscatter due to oceanic current shear and wind stress variations.* ESA contract report, 7997/88/F/F1, 51 pp.

JOHANNESSEN, J. A., R. A. SCHUCHMAN, O. M. JOHANNESSEN, K. L. DAVIDSON and D. R. LYZENGA. — 1991. Synthetic Aperture Radar imaging of upper ocean circulation features and wind fronts. *J. Geophys. Res.*, 96(C6): 10411-10422.

JOHANNESSEN, J. A., R. A. SCHUCHMAN, K. DAVIDSON, O. FRETTE, R. ONSTOTT and O. M. JOHANNESSEN. — 1992a. Coastal current studies with ERS-1 SAR during NORCSEX'91. *International Space Year Conference*, Munich, 5 pp.

JOHANNESSEN, J. A., L. P. ROED and T. WAHL. — 1992b. Eddies detected in ERS-1 SAR images and simulated in a reduced gravity model. *Int. J. Rem. Sensing* (accepted).

LA VIOLETTE, P. E., J. TINTORÉ and J. FONT. — 1990. The surface circulation in the Balearic Sea. *J. Geophys. Res.*, 95(C2): 1559-1568.

LEE, J. S. — 1981. Speckle analysis and smoothing of Synthetic Aperture Radar images. *Comp. Graph. Image Proces.*, 17: 24-32.

— 1983. A simple speckle smoothing algorithm for Synthetic Aperture Radar images. *IEEE Trans. Sys. Man. Cyber.*, SMC-13: 85-89.

LÓPEZ, M. J., C. MILLOT and J. FONT. — 1992. Circulación superficial en el Mar Balear durante el invierno a partir de imágenes NOAA-AVHRR. *IV Reun. Cient. Asoc. Esp. Teledet.*, Sevilla.

MARTÍNEZ, A., J. FONT and V. MORENO. — 1992. Análisis de imágenes SAR y su aplicación a estudios oceanográficos. *IV Reun. Cient. Asoc. Esp. Teledet.*, Sevilla.

SALAT, J., A. CASTELLÓN, J. SÁNCHEZ, J. FONT, A. JULIÁ, M. MANRÍQUEZ, M. I. LLORET, A. VIÚDEZ, J. MOLERO, J. MERINO and T. C. WILSON. — 1992. The interaction between the Catalan and Balearic currents in the southern Catalan Sea. FE91 cruise (May 1991). *Rapp. Comm. Int. Mer Médit.*, 33.

SATMER. — 1991. *Bulletin Mensuel de Renseignements Océanographiques Obtenus à Partir de Mesures Satellitaires Météorologiques sur la Méditerrannée et l'Atlantique Nord-Est*, Direction de la Météorologie Nationale, France, 98.

TINTORÉ, J., D. P. WANG and P. E. LA VIOLETTE. — 1990. Eddies and thermohaline intrusions on the shelf/slope front off the NE Spanish coast. *J. Geophys. Res.*, 95(C2): 1627-1634.

ULABY, F. T., R. K. MOORE and A. K. FUNG. — 1986. *Microwave Remote Sensing.* vol II: *Radar Remote Sensing and Surface Scattering and Emission Theory.* Artech House, Nordwood, USA.

VALENZUELA, G. R. — 1978. Theories for the interaction of electromagnetic and oceanic waves- A review. *Boundary Layer Meteorol.*, 13: 61-85.

VESECKY, J. F. and R. H. STEWART. — 1982. The observation of ocean surface phenomena using imagery from SEASAT SAR: An assessment. *J. Geophys. Res.*, 87: 3397-3430.

WANG, D. P., M. VIEIRA, J. SALAT, J. TINTORÉ and P. E. LA VIOLETTE. — 1988. A shelf/slope frontal filament off the Northeast Spanish coast. *J. Mar. Res.*, 46(2): 321-332.

WRIGHT, J. W. — 1978. Detection of ocean waves by microwave radar: The modulation of short gravity-capillary waves. *Boundary Layer Meteorol.*, 13: 87-105.

Scient. ed. P. E. La Violette.